Effect of Noble Metal Addition
on Co_3O_4-Based Gas Sensors for Selective NO Detection

Takafumi Akamatsu,* Toshio Itoh, Noriya Izu, and Woosuck Shin

National Institute of Advanced Industrial Science and Technology (AIST),
Inorganic Functional Materials Research Institute, 2266-98, Anagahora,
Shimo-Shidami, Moriyama, Nagoya, Aichi 463-8560, Japan

P-type semiconductor-based gas sensors have been fabricated for the selective detection of 50–200 ppb nitric oxide (NO). To fabricate the sensors, cobalt oxide (Co_3O_4) powders containing a noble metal (Pd, Ag, Pt, or Au) at 10 wt% were prepared by a colloidal mixing method and deposited on interdigitated Pt electrodes. The sensing responses to 50 and 200 parts per billion (ppb) NO and 25 and 100 parts per million (ppm) H_2 in air were investigated. The sensors with 10 wt% Pd, Ag, Pt, or Au loaded on the Co_3O_4 powder demonstrated a greater response to NO than Co_3O_4 with no noble metal content. The addition of Ag was found to suppress the H_2 response, a phenomenon that is attributed to the surface modification effects of Ag on the Co_3O_4 surface. Furthermore, the sensor with 5 wt% Pd and 5 wt% Ag loaded on the Co_3O_4 showed a high response in the presence of 50 ppb NO, as well as good selectivity against H_2.

1. Introduction

Human breath includes small amounts of biomarker gases, such as hydrogen (H_2), nitric oxide (NO), carbon monoxide (CO), methane (CH_4), and various volatile organic components (VOCs), at low concentrations in the range from several parts per billion (ppb) to parts per million (ppm).[1–3] NO concentration in human breath is associated with airway inflammatory disorders such as asthma and bronchiectasis.[4–6] Although monitoring NO concentration in human breath is one of the best noninvasive screening tests for the early diagnosis of these inflammatory disorders, this screening process requires an analytic device with sufficient accuracy at the ppb level.

Semiconductor gas sensors based on metal oxides have been considered as promising candidates for NO measurement because of their low cost, compact size, and direct electronic interface.[7–11] Among the metal oxides, n-type tungsten oxide (WO_3) appears to be a promising material for use in a NO gas sensor.[8,9] In a previous publication, we reported on the reliable response of a p-type cobalt oxide (Co_3O_4) gas sensor to NO gas at 0.5–5 ppm in air.[10] Furthermore, because that Co_3O_4 gas sensor showed a low resistance of below 1 kΩ, the peripheral circuit used to measure the sensor resistance does not require a large resistance, reducing the device cost. However, to the best of our knowledge, the Co_3O_4-based gas sensor's responses to NO gas at several hundred ppb have not been studied. In the case of breath analysis, sensors for the detection of NO concentrations in the range

---

*Corresponding author: e-mail: t-akamatsu@aist.go.jp

from several ten to several hundred ppb require selectivity against other gases such as H_2, CO, CH_4, and VOCs. The H_2 concentration level in human breath has been measured at the several tens of ppm level, and it exists at higher concentrations than the other gases.[12] Moreover, the Co_3O_4-based gas sensor in our previous publication showed a low response even at 0.5 ppm NO, and responses to NO gas at several hundred ppb have not been studied.[10] Therefore, the addition of a noble metal to these metal oxide semiconductors is critical for improving the sensitivity and selectivity of these gas sensors.[13,14]

We reported that the NO gas sensing properties of the Pd-loaded Co_3O_4 sensor with 0.1–30 wt% Pd content were estimated and the sensor with 10 wt% Pd content showed a high response and signal-to-noise ratio.[15] In this study, Co_3O_4 powder with 10 wt% noble metal (Pd, Ag, Pt, and Au) content was prepared by the colloidal mixing method, and the responses of these sensors to 50 and 200 ppb NO in air were investigated, in reference to the response of a sensor based on pure Co_3O_4.[14,15] To discuss the selectivity against other gases as an initial evaluation, their responses to H_2 in air were also investigated.

2. Materials and Methods

Five distinct colloidal suspensions were prepared by mixing commercial Co_3O_4 powder (Sigma-Aldrich) with 10 wt% Pd, 10 wt% Ag, 10 wt% Pt, 10 wt% Au, and 5 wt% Pd + 5 wt% Ag particles. "10 wt% Pd" means that the total Pd content is 10 wt% in the powder. The particle size of the Co_3O_4 powder was 20–30 nm, and the average particle sizes of the Pd, Ag, Pt, and Au in the colloidal suspension (Tanaka Kikinzoku Kogyo K.K.) were approximately 4, 15, 2, and 3 nm, respectively.

The Co_3O_4 powder was stirred in an ethanol solution, followed by the addition of the Pd, Ag, Pt, or Au colloidal suspension. Subsequently, the solution was stirred at 70 °C until the ethanol evaporated. The resulting solid residue was baked in air at 400 °C for 2 h to make a sensing material powder with 10 wt% metal content. A ceramic paste of the sensing material powder was prepared by mixing an organic dispersant consisting of 10 wt% ethyl cellulose and 90 wt% terpineol. The weight ratio of the sensing material powder to the organic dispersant was 1:16. The paste was dispensed on a surface-oxidized Si substrate consisting of 2.5 × 4 mm^2 Pt interdigital electrodes with line and space definitions of 15 μm each. These units were then baked in air at 400 °C for 2 h to produce sensors with sensing membranes of 2–6 μm thickness on the Si substrate. A pure Co_3O_4 sensor was also prepared in a similar manner. Figure 1 shows a schematic illustration of the sensor.
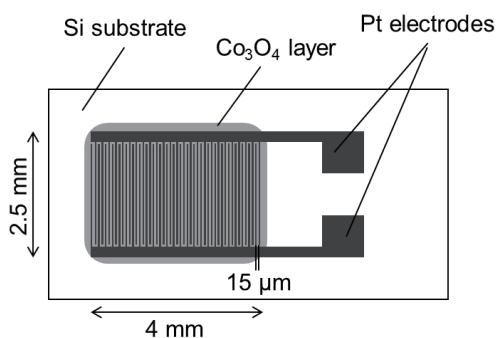

Fig. 1.   Schematic illustration of the sensor.

The sample powders were characterized by X-ray diffraction (XRD) analysis and transmission electron microscopy (TEM). The XRD analysis was carried out using a Smartlab diffractometer (Rigaku Corporation) equipped with a copper source (CuKα) and a one-dimensional high-speed detector (D/teX Ultra 250). The X-ray generator was operated at 40 kV and 30 mA. The TEM analysis was performed using a JEM-2010 instrument (JEOL Ltd.).

The NO gas responses of the sensors were investigated using a flow test chamber heated to 100–300 °C in an electrical tube furnace. After placing a sensor in the chamber, air and NO in air were allowed to flow into the chamber alternately, at a flow rate of 200 mL/min. Air and NO in air were prepared by mixing with 99.99% N_2 gas, N_2-balanced 10 ppm NO gas, and 99.5% O_2 gas. The O_2 content in air and NO in air was 20 vol%. The NO concentration was controlled to the values of 0, 50, and 200 ppb in air. The sensor resistance in various gaseous atmospheres was measured by a two-probe method at 10 s intervals using a K2700 digital multimeter (Keithley). We defined the sensor response value (S) using the following equation: $S = R_g/R_a$, where R_g denotes the resistance after 15 min of NO gas exposure, and R_a denotes the resistance in air prior to NO gas exposure.

The response of the sensors to H_2 gas was investigated using the same apparatus as was used to measure the NO gas response. The H_2 gas concentration was controlled to the values of 0, 25, and 100 ppm in air.

3. Results and Discussion

Figures 2(a)–2(e) show the XRD patterns of the pure Co_3O_4, Co_3O_4 + 10 wt% Pd, Co_3O_4 + 10 wt% Ag, Co_3O_4 + 10 wt% Pt, and Co_3O_4 + 10 wt% Au powders, respectively, after baking at 400 °C for 2 h. No structural changes, such as the decomposition and oxidation of Co_3O_4, were observed after baking at 400 °C for 2 h because Co_3O_4 peaks (JCPDS card no. 74-2120) were observed at
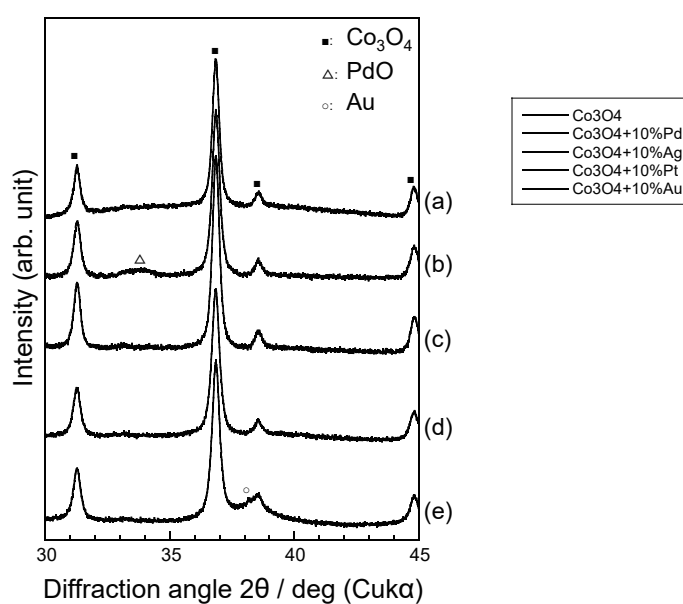

Fig. 2.   XRD patterns of (a) pure Co_3O_4, (b) Co_3O_4 + 10 wt% Pd, (c) Co_3O_4 + 10 wt% Ag, (d) Co_3O_4 + 10 wt% Pt, and (e) Co_3O_4 + 10 wt% Au powders, after baking at 400 °C for 2 h.

31.2, 36.8, 38.5, and 44.8°. In Fig. 2(b), a small broad peak at 33.8° was observed in the pattern of the Co_3O_4 sensor loaded with 10 wt% Pd. This pattern was assigned to PdO (JCPDS card no. 75-0584), and is attributed to the oxidation of Pd to PdO during the baking at 400 °C for 2 h. In Fig. 1(e), a peak with a broad width was observed at 38.2° in the pattern of the sensor loaded with 10 wt% Au. This peak was assigned to Au (JCPDS card no. 04-0784). No other peaks were observed in the patterns of the sensors loaded with 10 wt% Ag or 10 wt% Pt. The crystallite sizes (D) were calculated using the Scherrer equation $D = k\lambda/\beta\cos\theta$, where k (= 0.94) is the shape factor, λ is the X-ray wavelength, β is the full width of the diffraction peak at half its maximum, and θ is the Bragg diffraction angle. The D values of the Co_3O_4 peaks at 36.8° in pure Co_3O_4, Co_3O_4 +10 wt% Pd, Co_3O_4 + 10 wt% Ag, Co_3O_4 + 10 wt% Pt, and Co_3O_4 + 10 wt% Au were estimated to be 29.5, 25.8, 28.2, 24.7, and 26.6 nm, respectively. These D values are almost comparable to the Co_3O_4 particle size of 20–30 nm.

Figures 3(a)–3(e) show TEM images of pure Co_3O_4, Co_3O_4 + 10 wt% Pd, Co_3O_4 + 10 wt% Ag, Co_3O_4 + 10 wt% Pt, and Co_3O_4 + 10 wt% Au powders, respectively, after baking at 400 °C for 2 h. Pale phases, which are Co_3O_4 particles, can be observed in Figs. 3(a)–3(e). In addition, dark phases of approximately 30 nm diameter can be observed in Fig. 3(c), and dark phases of approximately 5 nm diameter can be observed in Figs. 3(d) and 3(e). These dark phases are considered to be the metal particles. No dark phases are apparent in the image of the sensor loaded with 10 wt% Pd in Fig. 3(b); this is attributed to the phenomenon reported by Matsushima *et al.*,[16] in which PdO particles on a SnO_2 surface were reported to be less visible in TEM images. Because the Pd in the powder existed as PdO, it showed less contrast to Co_3O_4, and therefore, it was indistinguishable from the Co_3O_4 in the TEM image. We used Pd, Ag, Pt, and Au because of their dispersion properties in colloidal solutions. It is observed from Fig. 3 that the metal nanoparticles are bonded with the Co_3O_4 particles without obvious aggregation, even though the metal weight ratio is 10 wt%.
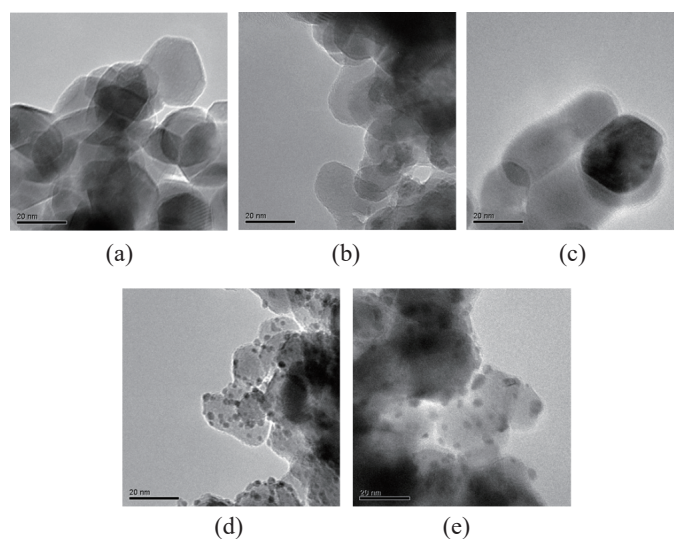

Fig. 3. TEM images of (a) pure Co_3O_4, (b) Co_3O_4 + 10 wt% Pd, (c) Co_3O_4 + 10 wt% Ag, (d) Co_3O_4 + 10 wt% Pt, and (e) Co_3O_4 + 10 wt% Au powders, after baking at 400 °C for 2 h.

Figures 4(a)–4(e) show the responses of the sensors with pure Co_3O_4, Co_3O_4 + 10 wt% Pd, Co_3O_4 + 10 wt% Ag, Co_3O_4 + 10 wt% Pt, and Co_3O_4 + 10 wt% Au powders, respectively, during exposure to 0, 50, and 200 ppb NO in air at 100 °C. When all sensors were exposed to the NO gas, the sensor resistances began to increase. Because the majority carrier of the Co_3O_4 is the hole, the holes combine with electrons, and the hole concentration at the Co_3O_4 surface decreases, resulting in the increasing resistance of the Co_3O_4.[17] When Co_3O_4 is exposed to air, the O_2 absorbed on the Co_3O_4 surface, resulting in the formation of absorbed oxygen ions (O_2^-, O^{2-}, or O^-). When a reductive NO gas flows onto the Co_3O_4, the NO gas combines with adsorbed oxygen ions at the Co_3O_4 surface, releasing electrons back to the conduction band. Therefore, the resistance of the sensors increased with increasing exposure to NO gas. All the sensors showed a distinct response to the NO gas, even at 50 ppb. The sensor resistance was higher in the presence of 200 ppb NO than in the presence of 50 ppb NO. In Fig. 4(a), the resistance of the pure Co_3O_4 membrane exposed to 50 ppb NO did not return to R_a, even after 15 min of air exposure. This result shows that adsorbed NO on the pure Co_3O_4 membrane surface did not desorb from the surface during the 15 min of 0 ppb NO air exposure. On the other hand, the resistance of the Co_3O_4 membranes loaded with Pd, Ag, Pt, and Au decreased after 15 min of 0 ppb NO air exposure, relative to the resistance of the pure Co_3O_4 membrane. In the case of the pure Co_3O_4, it is possible that diffusing NO molecules do not undergo sufficient oxidation and are adsorbed on the surfaces of the Co_3O_4 particles. The magnitude of the increase in the resistance of the Co_3O_4-based sensors would be affected by the density of carrier electrons from the combustion of NO molecules and the associated consumption of adsorbed O^{2-} on the Co_3O_4 surface. This suggests that the loaded noble metals promote the combustion of NO molecules during NO gas exposure and the adsorption of O_2 on the Co_3O_4 surface during 0 ppb NO air exposure.
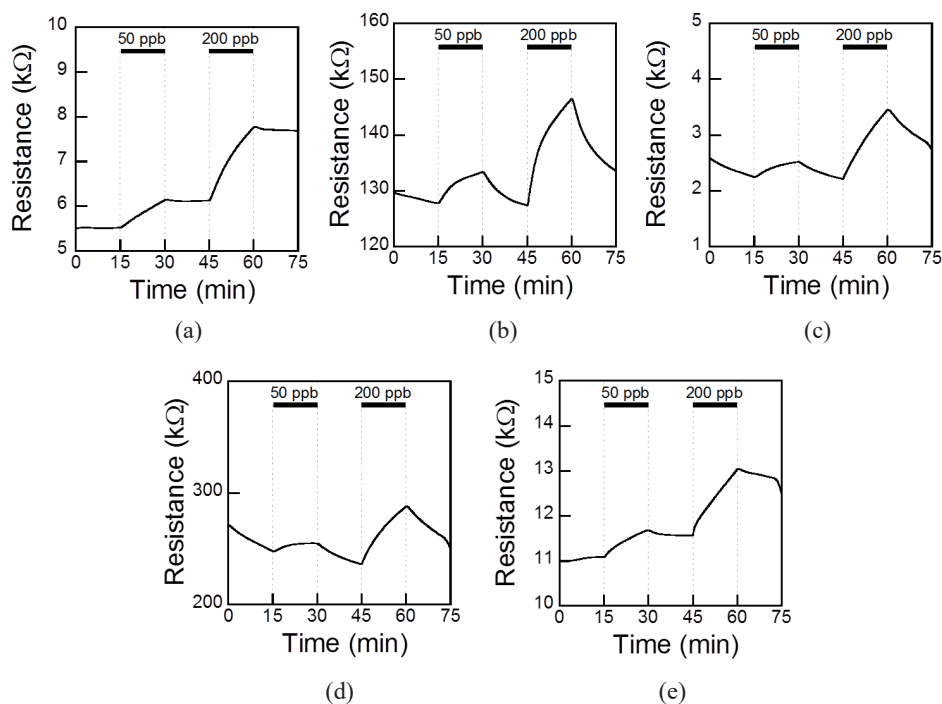

Fig. 4.   Responses of the sensor with (a) pure Co_3O_4, (b) Co_3O_4 + 10 wt% Pd, (c) Co_3O_4 + 10 wt% Ag, (d) Co_3O_4 + 10 wt% Pt, and (e) Co_3O_4 +10 wt% Au powders, during exposure to 0, 50, and 200 ppb NO in air at 100 °C.

Figures 5(a)–5(e) and 6(a)–6(e) show the responses of the sensors with pure Co_3O_4, Co_3O_4 + 10 wt% Pd, Co_3O_4 + 10 wt% Ag, Co_3O_4 + 10 wt% Pt, and Co_3O_4 + 10 wt% Au powders, respectively, during exposure to 0, 50, and 200 ppb NO in air at 200 and 300 °C, respectively. The resistances of all the sensors increased during exposure to 50 and 200 ppb NO gas at both 200 and 300 °C. In addition, the resistance of NO⁻exposed sensors decreased during exposure to 0 ppb NO air. The time required to return to 90% of the steady-state value of R_a or R_g decreased with increasing operating temperatures. This suggests that increasing operating temperatures promoted the combustion of NO molecules or the adsorption of O_2 on the Co_3O_4 surface. Figures 7(a)–7(e) show sensing responses to the 50 and 200 ppb NO of the sensors with pure Co_3O_4, Co_3O_4 + 10 wt% Pd, Co_3O_4 + 10 wt% Ag, Co_3O_4 + 10 wt% Pt, and Co_3O_4 + 10 wt% Au powders, respectively, as a function of operating temperature. The high sensor responses, $S_{NO} = R_g/R_a$, of the pure Co_3O_4, Co_3O_4 + 10 wt% Pd, Co_3O_4 + 10 wt% Ag, Co_3O_4 + 10 wt% Pt, and Co_3O_4 + 10 wt% Au sensors toward 50 ppb NO were estimated to be 1.11, 1.16, 1.12, 1.12, and 1.09 at 100, 200, 100, 200, and 200 °C, respectively. The Pd-loaded Co_3O_4 sensor showed the highest response toward 50 ppb NO. In the case of the 200 ppb NO concentration, the highest response of $S_{NO} = 1.54$ was obtained with the Ag-loaded Co_3O_4 sensor at 100 °C. The sensor responses to NO at 300 °C were smaller than their responses at 100 and 200 °C. In Figs. 4–6, the sensor response rate at 100 °C was lower than the sensor response rate at 200 and 300 °C. Therefore, the optimum operating temperature was approximately 200 °C.
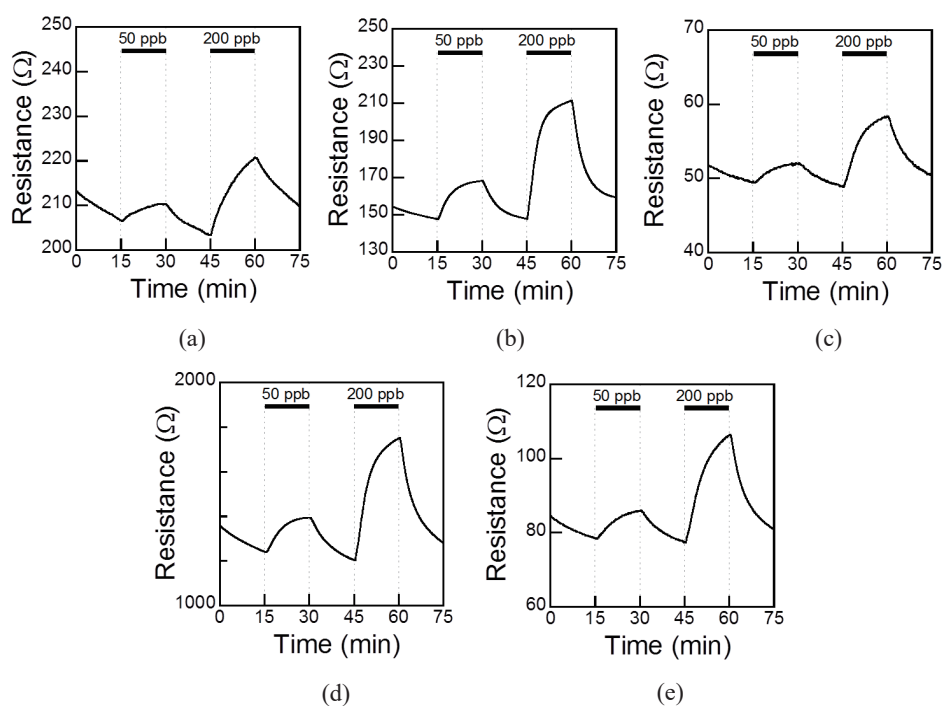

Fig. 5.   Responses of the sensor with (a) pure Co_3O_4, (b) Co_3O_4 +10 wt% Pd, (c) Co_3O_4+ 10 wt% Ag, (d) Co_3O_4 + 10 wt% Pt, and (e) Co_3O_4 + 10 wt% Au powders, during exposure to 0, 50, and 200 ppb NO in air at 200 °C.
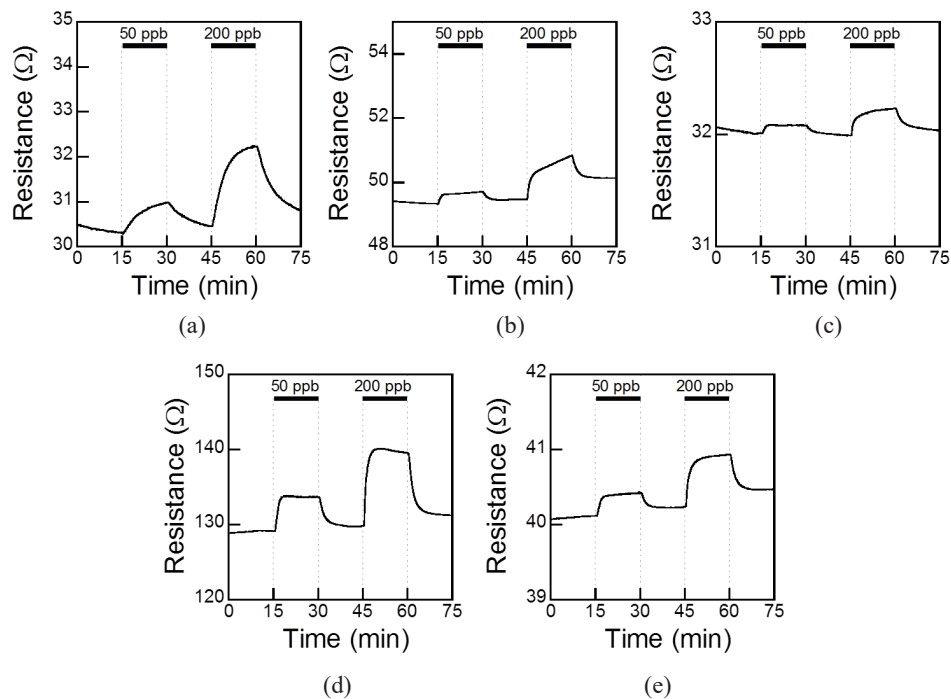
Fig. 6.   Responses of the sensor with (a) pure Co_3O_4, (b) Co_3O_4 + 10 wt% Pd, (c) Co_3O_4 + 10 wt% Ag, (d) Co_3O_4 + 10 wt% Pt, and (e) Co_3O_4 + 10 wt% Au powders, during exposure to 0, 50, and 200 ppb NO in air at 300 °C.
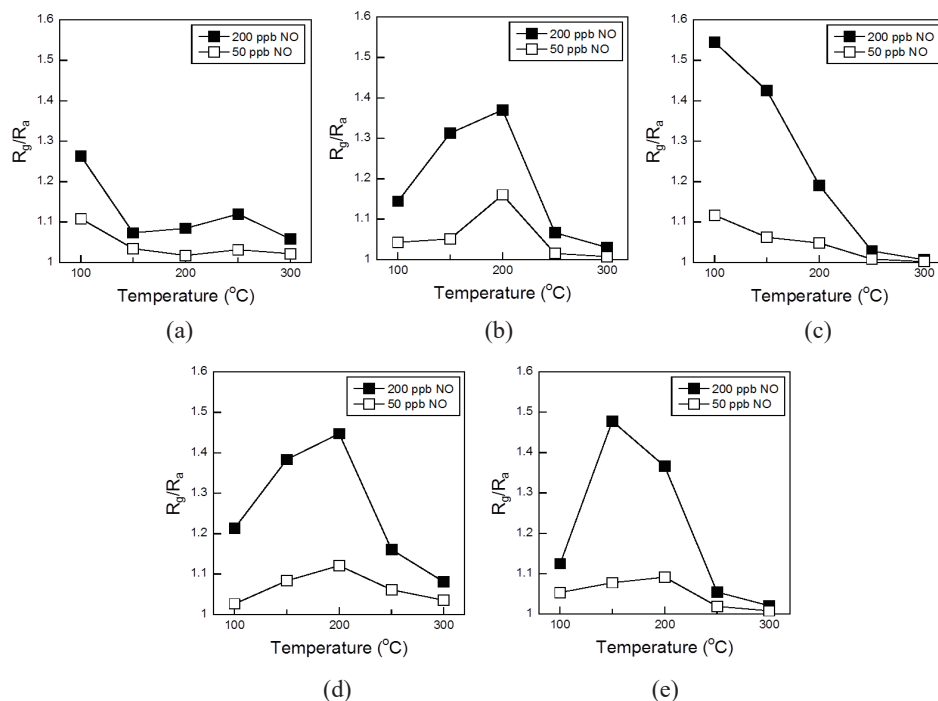
Fig. 7.   Sensing responses of the sensor with (a) pure Co_3O_4, (b) Co_3O_4 + 10 wt% Pd, (c) Co_3O_4 + 10 wt% Ag, (d) Co_3O_4 + 10 wt% Pt, and (e) Co_3O_4 + 10 wt% Au powders, to 50 and 200 ppb NO as a function of operating temperature.

Unlike the other metal-loaded Co_3O_4 sensors, the sensing response of the Ag-loaded Co_3O_4 sensor decreased with increasing operating temperature. This is attributed to the difference in the metal particle size, because the Ag particle is larger than the Pd, Pt, and Au particles. This relationship between the sensing response and the size of the metal particle will be investigated in the future.

Figure 8 shows the sensor resistances of the pure Co_3O_4, Co_3O_4 + 10 wt% Pd, Co_3O_4 + 10 wt% Ag, Co_3O_4 + 10 wt% Pt, and Co_3O_4 + 10 wt% Au powders in air as a function of temperature. To determine each sensor's resistivity or conductivity, the thickness and porosity of each sensor's membrane should be estimated as precisely as possible. This is difficult to perform with sufficient accuracy, and we therefore plotted only the resistance in air (R_a) on the vertical axis. However, the temperature dependences of the resistance and resistivity are the same. Figure 8 shows decreasing resistance with increasing operating temperature. The resistance of the Co_3O_4 membrane increased with the addition of Pd and increased even more with the addition of Pt. This increase in the sensor resistance is probably caused by a decrease in the hole concentration at the Co_3O_4 surface. On the other hand, the addition of Ag or Au was not expected to cause a decrease in the hole concentration. The resistance of the Ag- or Au-loaded Co_3O_4 membrane was slightly smaller than that of the pure Co_3O_4 membrane. It is assumed that Ag or Au in the sensor membrane has not only some surface modification effects that enhance the sensor response, but also a conductive effect connecting the Co_3O_4 particles and decreasing the sensor resistance.

When the sensors were exposed to H_2 gas, the resistances of all the sensors increased. The H_2 sensor responses (S_{H2}) were estimated using $S_{H2} = R_g/R_a$. Figures 9(a)–9(e) show the responses of the sensors with pure Co_3O_4, Co_3O_4 + 10 wt% Pd, Co_3O_4 + 10 wt% Ag, Co_3O_4 + 10 wt% Pt, and Co_3O_4 + 10 wt% Au powders, respectively, to the 25 and 100 ppm H_2 as a function of operating temperature. The highest response of the sensor with pure Co_3O_4 was $S_{H2} = 1.37$ at 200 °C for 100 ppm H_2 exposure. On the other hand, the highest responses of the sensors with the Co_3O_4 loaded
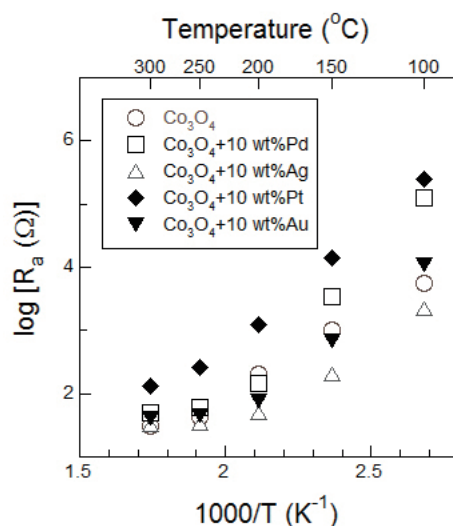

Fig. 8.   Resistances of the sensor with pure Co_3O_4, Co_3O_4 + 10 wt% Pd, Co_3O_4 + 10 wt% Ag, Co_3O_4 +10 wt% Pt, and Co_3O_4 + 10 wt% Au powders, in air as a function of operating temperature.
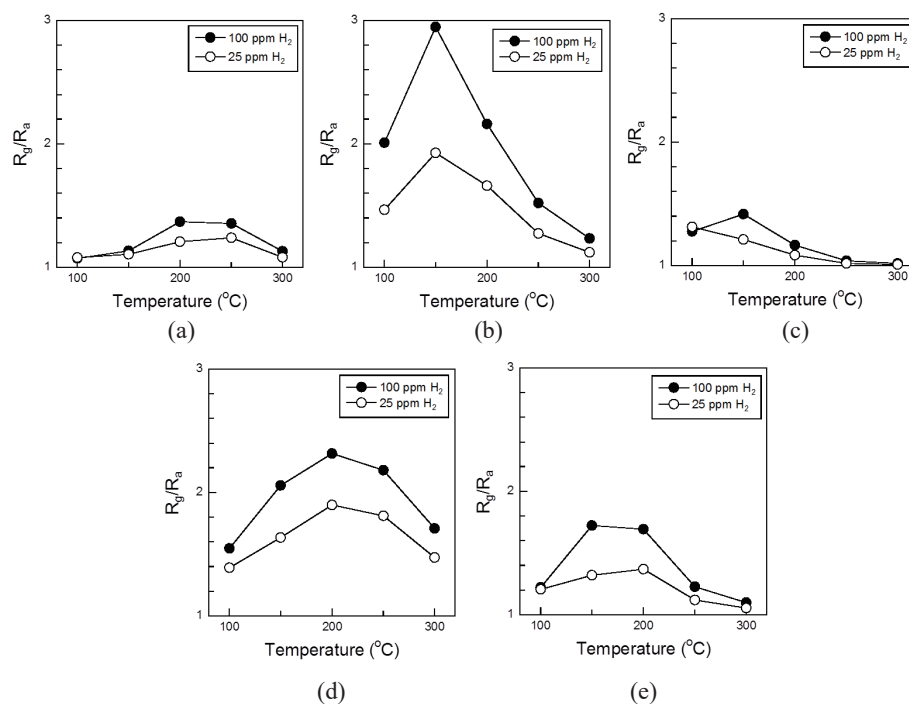
Fig. 9.   Sensing responses of the sensor with (a) pure Co_3O_4, (b) Co_3O_4 + 10 wt% Pd, (c) Co_3O_4 + 10 wt% Ag, (d) Co_3O_4 + 10 wt% Pt, and (e) Co_3O_4 + 10 wt% Au powders, to 25 and 100 ppm H_2 as a function of operating temperature.

with 10 wt% Pd, 10 wt% Ag, 10 wt% Pt, and 10 wt% Au were S_{H2} = 2.95 at 150 °C, S_{H2} = 1.42 at 150 °C, S_{H2} = 2.32 at 200 °C, and S_{H2} = 1.72 at 150 °C, respectively, for 100 ppm H_2 exposure. These results show that the level of H_2 gas present in human breath interferes with the NO responses of these Co_3O_4-based sensors. Moreover, the Co_3O_4-based sensors may respond to other gases, such as oxidizing gases (such as NO_2 and CO_2), reducing gases (such as CO and CH_4), H_2O, and VOCs. When the sensor is exposed to a oxidizing gas, the resistance of the sensor decreased. [17] On the other hand, when the sensor is exposed to H_2O and VOCs, the sensor response is reported to be inaccurate.[18] Therefore, the Co_3O_4-based sensor must include a gas separation filter to remove the interference from gases such as NO_2, CO_2, CH_4, CO, H_2O, and VOCs.

   Among the noble-metal-loaded Co_3O_4-based sensors, the Ag-loaded sensor showed lower responses toward 25 and 100 ppm H_2 than the others. From this result, the Ag-loaded Co_3O_4 sensor is considered to demonstrate good selectivity against H_2 gas. Yamazoe *et al.* reported that the gas behaviors of $Pd-SnO_2$ and $Pt-SnO_2$ were controlled by a chemical interaction in which noble metals assist the redox processes of the semiconductor, and the gas behavior of $Ag-SnO_2$ was controlled by an electronic interaction in which noble metals interact electronically with the semiconductor as an electron donor or acceptor.[13] The selectivity against H_2 gas may be affected by the different surface modification effects of the various noble metals on the Co_3O_4-based sensor membrane.

   To improve the sensor response to NO, further investigation is required to detect sub-ppb levels of NO with sufficient accuracy. Sakai et al. have reported that the multiple-noble-metal (Pd, Pt, and Au)-loaded SnO_2 showed higher sensor response toward VOCs than a single-noble-metal-loaded
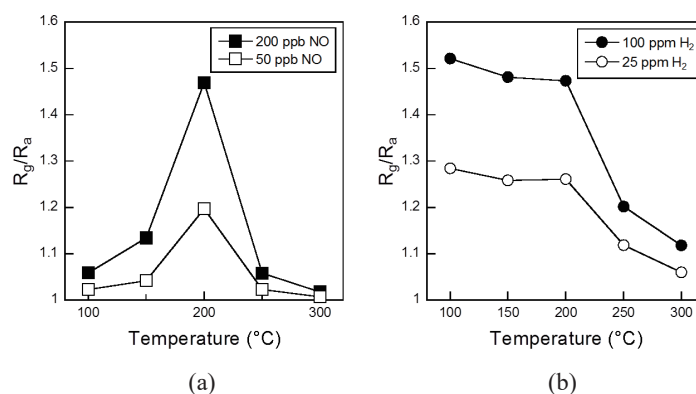
Fig. 10. Sensing responses of the sensor with Co_3O_4 loaded with 5 wt% Pd and 5 wt% Ag powders to (a) 50 and 200 ppb NO, and (b) 25 and 100 ppm H_2, as a function of operating temperature.

SnO_2.[19] To estimate the effects of multiple noble metal loadings, we investigated the responses of the Pd/Ag-loaded Co_3O_4 sensor because the Pd-loaded Co_3O_4 sensor showed the highest response toward 50 ppb NO, and the Ag-loaded Co_3O_4 sensor showed the lowest response toward 100 ppm H_2. Figures 10(a) and 10(b) show the responses of the Co_3O_4 sensor loaded with 5 wt% Pd and 5 wt% Ag powders toward NO and H_2 as a function of operating temperature. The high responses were S_{NO} = 1.20 and 1.47 for 50 and 200 ppb NO, respectively, at 200 °C. In addition, the responses for 25 and 100 ppm H_2 were S_{H2} = 1.26 and 1.47, respectively, at 200 °C. The Co_3O_4 sensor loaded with 5 wt% Pd and 5 wt% Ag showed a higher NO response and a lower H_2 response than the Co_3O_4 sensors loaded with a single noble metal. To enhance these sensor properties, the optimization of the doping ratio of Pd to Ag and Co_3O_4 sensors loaded with multiple noble metals will be further investigated in the future.

4.   Conclusions

In this study, NO gas sensors based on Co_3O_4 as a sensitive functional material were manufactured, and their sensing properties were investigated. The sensors with 10 wt% noble metal (Pd, Ag, Pt, or Au) require less time to return to 90% of the steady-state values of R_a or R_g and have higher responses toward NO gas than Co_3O_4-based sensors with no noble metal content. Among the noble-metal-loaded Co_3O_4 sensors, the sensor loaded with 10 wt% Ag content demonstrated good selectivity against H_2 gas. The Co_3O_4 sensor loaded with 5 wt% Pd and 5 wt% Ag showed better NO response and lower H_2 response than the Co_3O_4 sensors loaded with a single noble metal.

References

1   K. M. Behall, D. J. Scholfield, A. M. van der Sluijs, and J. Hallfrisch: J. Nutr. **128** (1998) 79.
2   M. T. Roberge, J. W. Finley, H. C. Lukaski, and A. J. Borberding: J. Chromatogr. A **1027** (2004) 19.
3   P. Fuchs, C. Loeseken, J. K. Schubert, and W. Miekisch: Int. J. Cancer **126** (2010) 2663.
4   J. Saito, K. Inoue, A. Sugawara, M. Yoshikawa, K. Watanabe, T. Ishida, Y. Ohtsuka, and M. Munakata: J. Allergy. Clin. Immunol. **114** (2004) 512.
5   T. Grzelewski, M. Paweł, J. Joanna, C. Łukasz, K. Jan, S. Włodzimierz, S. Rafał, J. Anna, G. Aleksandra, and S. Iwona: Nitric Oxide **25** (2011) 288.

6   F. M. Delen, J. M. Sippel, M. L. Osborne, A. Law, N. Thukkani, and W. E. Holden: Chest **117** (2000) 695.
7   T. Ishihara, K. Shiokawa, K. Eguchi, and H. Arai: Sens. Actuators **19** (1989) 259.
8   M. Akiyama, J. Tamaki, N. Miura, and N. Yamazoe: Chem. Lett. **20** (1991) 1611.
9   M. Penza, C. Martucci, and G. Cassano: Sens. Actuators, B **50** (1998) 52.
10 T. Akamatsu, T. Itoh, N. Izu, and W. Shin: Sensors **13** (2013) 12467.
11 C. Sun, G. Maduraiveeran, and P. Dutta: Sens. Actuators, B **186** (2013) 117.
12 W. Shin: Anal. Bioanal. Chem. **406** (2014) 3931.
13 N. Yamazoe, Y. Kurokawa, and T. Seiyama: Sens. Actuators **4** (1983) 283.
14 T. Itoh, T. Nakashima, T. Akamatsu, N. Izu, and W. Shin: Sens. Actuators, B **187** (2013) 135.
15 T. Akamatsu, T. Itoh, N. Izu, W. Shin, and K. Sato: Sensors **15** (2015) 8109.
16 S. Matsushima, J. Tamaki, N. Miura, and N. Yamazoe: Chem. Lett. **18** (1989) 1651.
17 K. Wetchakun, T. Samerjai, N. Tamaekong, C. Liewhiran, C. Siriwong, V. Kruefu, A. Wisitsoraat, A. Tuantranont, and S. Phanichphant: Sens. Actuators, B **160** (2011) 580.
18 G. F. Fine, L. C. Cavanagh, A. Afonja, and R. Binions: Sensors **10** (2010) 5469.
19 Y. Sakai, M. Kadosaki, I. Matsubara, and T. Itoh: J. Ceram. Soc. Jpn. **117** (2009) 1297.